Taylor & Francis
Taylor & Francis Group

Computer Methods in Biomechanics and Biomedical Engineering

ISSN: 1025-5842 (Print) 1476-8259 (Online) Journal homepage: http://www.tandfonline.com/loi/gcmb20

# Triphasic mixture model of cell-mediated enzymatic degradation of hydrogels

Franck J. Vernerey , Eric C. Greenwald & Stephanie J. Bryant

**To cite this article:** Franck J. Vernerey , Eric C. Greenwald & Stephanie J. Bryant (2012) Triphasic mixture model of cell-mediated enzymatic degradation of hydrogels, Computer Methods in Biomechanics and Biomedical Engineering, 15:11, 1197-1210, DOI: 10.1080/10255842.2011.585973

**To link to this article:** https://doi.org/10.1080/10255842.2011.585973

*Computer Methods in Biomechanics and Biomedical Engineering*
Vol. 15, No. 11, November 2012, 1197–1210

Taylor & Francis
Taylor & Francis Group

# Triphasic mixture model of cell-mediated enzymatic degradation of hydrogels

Franck J. Vernerey[a1]*, Eric C. Greenwald[b1] and Stephanie J. Bryant[b]

[a]*Department of Civil, Environmental and Architectural Engineering, University of Colorado, Boulder, CO, USA;* [b]*Department of Chemical and Biological Engineering, University of Colorado, Boulder, CO, USA*

(*Received 21 September 2010; final version received 3 May 2011*)

One critical component of engineering living tissue equivalents is the design scaffolds (often made of hydrogels) whose degradation kinetics can match that of matrix production by cells. However, cell-mediated enzymatic degradation of a hydrogel is a highly complex and nonlinear process that is challenging to comprehend based solely on experimental observations. To address this issue, this study presents a triphasic mixture model of the enzyme–hydrogel system, which consists of a solid polymer network, water and enzyme. On the basis mixture theory, the rubber elasticity theory and the Michaelis–Menton kinetics for degradation, the model naturally incorporates a strong coupling between gel mechanical properties, the kinetics of degradation and the transport of enzyme through the gel. The model is then used to investigate the particular problem of a single spherical enzyme-producing cell, embedded in a spherical hydrogel domain, for which the governing equations can be cast within the cento-symmetric assumptions. The governing equations are subsequently solved using an implicit nonlinear finite element procedure to obtain the evolution of enzyme concentration and gel degradation through time and space. The model shows that two regimes of degradation behaviour exist, whereby degradation is dominated either by diffusion or dominated by reaction kinetics. Depending on the enzyme properties and the initial hydrogel design, the temporal and spatial changes in gel cross-linking are dramatically impacted, a feature that is likely to strongly affect new tissue development.

**Keywords:** multiphasic model; hydrogel degradation; tissue engineering

## 1. Introduction

Tissue engineering aspires to develop functional tissue equivalents using a combination of cells, scaffolds and/or external biochemical or biomechanical stimuli. One strategy that has gained significant attention is the encapsulation of cells within highly water swollen cross-linked polymeric networks (i.e. hydrogels). Hydrogels are particularly attractive because they mimic the high water content of tissues, present a 3D environment to the cells which is critical to their function and permit facile transport of nutrients to the cells and waste from the cells. Furthermore, many strategies have been designed to permit *in vivo* polymerisation and/or cross-linking enabling the delivery of cells *in vivo* using minimally invasive procedures (Elisseeff et al. 1999; Shu et al. 2006). In an effort to tailor the 3D environment towards a specific tissue, numerous natural and synthetic chemistries as well as degradation schemes have been examined (Nicodemus and Bryant 2008). Although many natural hydrogels provide biological recognition to the cells and are able to be remodelled by the cell via cell-secreted enzymes, they have limited tailorability and are often mechanically inferior. Recent efforts have focused on designing synthetic hydrogels with biological moieties to capture the attractive features of natural hydrogels, but which can be fabricated to exhibit a range of macroscopic properties (Lutolf and Hubbell 2005; Tibbitt and Anseth 2009). One attractive strategy is to incorporate oligopeptides, which contain the cleavage site recognised by matrix degrading enzymes (e.g. matrix metalloproteinases or MMPs), into the cross-links of synthetic hydrogels (Gobin and West 2002; Lutolf et al. 2003; Levesque and Shoichet 2007). In this scheme, cells dictate hydrogel degradation.

Several studies have demonstrated the success of enzymatically degradable hydrogels. For example, when cell adhesion moieties were programmed into a hydrogel-containing enzymatically susceptible cross-links, cell-mediated degradation enabled cells to migrate through the hydrogel, a process that would otherwise be inhibited by the cross-linked network surrounding the cells (Gobin and West 2002; Lutolf et al. 2003; Lee et al. 2007) and enabled cell spreading, in which cells would otherwise remain rounded (Kim et al. 2008; Kraehenbuehl et al. 2008). Studies have also shown that a cell-mediated degradable hydrogel enhances matrix elaboration. For example, the pericellular matrix surrounding cartilage cells was more elaborate in MMP-sensitive hydrogels when compared with MMP-insensitive hydrogels (Park et al. 2004). Although many of the oligopeptide sequences represent the original cleavage sequence in the protein, slight changes in the amino acid sequence, such as exchanging one amino acid for another not normally present in the protein

*Corresponding author. Email: franck.vernerey@colorado.edu

ISSN 1025-5842 print/ISSN 1476-8259 online

http://dx.doi.org/10.1080/10255842.2011.585973
http://www.tandfonline.com

sequence, can dramatically impact the degradation kinetics. In this way, externally tuning the degradation behaviour of the hydrogel is also possible (Lutolf et al. 2003).

In designing a suitable hydrogel for encapsulating cells to regenerate living tissue, the degradation behaviour will have a large impact on how new matrix develops. In particular, the cross-linked structure largely dictates diffusion of new matrix and macroscopic tissue development (Bryant and Anseth 2001; Bryant and Anseth 2003). In hydrogels in which degradation is mediated locally by the cells, temporal changes in the cross-linked structure likely occur at and near the cell boundary. Lee et al. (2007) employed a collagenase-sensitive fluorogenic substrate as the cross-linker and confirmed that degradation occurred immediately surrounding the cell. However, the degree to which spatial changes in cross-linking occurs will depend on a number of factors including local enzyme concentration, the size of the enzyme relative to the mesh size of the hydrogel, the initial density of cross-links and the degradation kinetics. A better understanding of how these factors impact degradation behaviour in time and space would lead to improved hydrogel designs.

Numerical models typically offer a potential platform that can virtually guide the design of a wide class of materials by probing the effect of microstructural features on macroscopic observations (Vernerey et al. 2006, 2007a, 2007b). In particular, several models have been developed to describe the poromechanical behaviour for hydrated polymeric scaffolds and soft tissue. For example, Sun et al. (1999) derived a triphasic poromechanical model that describes ion flow within hydrogels and captures changes in the swelling properties. Sengers et al. (2004a, 2004b) have developed poromechanical models to describe transport of solutes in tissues subjected to dynamic loading. In these models, transport parameters and mechanical properties are constant throughout time. However, in degrading systems, these properties will certainly change. An alternative approach was described by Rice et al. (2006) who developed a statistical kinetic model to predict polymer mass loss from bulk degrading synthetic hydrogels. Their hydrogel system contained polycaprolactone within the cross-link, which can be degraded by exogenously delivering the enzyme, lipase. Using their model, the authors found that mass loss was highly dependent on the length of polycaprolactone and the lipase concentration. Although the above studies have provided precious information concerning either gel deformation and transport or gel degradation, none investigated their interactions in the present context. This gap in our knowledge is detrimental to current tissue engineering studies as these interactions are very likely to be major players in the cell-mediated gel degradation. The contribution of this paper is, therefore, to address this issue by (a) introducing a triphasic model that can characterise the combined effect of gel deformation, enzyme transport and gel degradation within a single framework, (b) deriving a numerical strategy to solve the resulting highly nonlinear problem and (c) numerically assessing different regimes of the cell-mediated gel degradation in terms of experimentally tunable parameters.

As stated above, the objective of this work was to derive a multiphasic poromechanical model capable of capturing the degradation behaviour of cell-mediated degradable hydrogels through space and time. To accurately capture the changes in mechanical and transport properties with gel degradation, the hydrogel network is modelled as a deformable porous network whereby the constitutive relationships are defined by rubber elasticity theory and equilibrium swelling theory of hydrogels (Peppas and Barr-Howell 1986; Bell and Peppas 1995). This approach is used to investigate the evolution of gel properties and deformation around a spherical cell releasing a constant enzyme flux. The resulting nonlinear partial differential equations (PDEs) are subsequently solved with a mixed finite element formulation. Using the data available in the literature, we describe the local and distant degradation behaviour of the hydrogel as a function of the size of enzyme molecules (relative to the hydrogel mesh size), initial cross-link density and degradation kinetics. Numerical simulations are then used to gain physical insight into the mechanisms driving cell-mediated hydrogel degradation behaviour. In particular, we show that there are two regimes of degradation behaviour, whereby degradation is dominated either by diffusion or by reaction kinetics. Depending on the enzyme properties and the initial hydrogel design, the temporal and spatial changes in gel cross-linking are dramatically impacted, a feature that is likely to strongly affect new tissue development.

## 2. Multiphasic formulation of enzymatically degrading hydrogel

Gel degradation mediated by enzymes involves a variety of phenomena including enzyme transport, disassembly of chemical bonds (resulting from gel–enzyme reaction) and gel swelling. The multiphysical behaviour of such solid–fluid mixtures has traditionally been described by the theory of porous media, originally introduced by Biot (1941, 1957) in the context of consolidation and later generalised to the theory of mixtures, notably by Trusdell and Noll (1965), and Bowen 1980. Extension of these theories to the interaction between multiple phases (solid, fluid and ions; Sun et al. 1999) has also been introduced, in particular to characterise the behaviour of hydrated tissues. These formulations were successful at capturing a number of complex phenomena in porous media including free swelling (Sun et al. 1999), osmosis and electro-osmosis or streaming potentials (Gu et al. 1999).

The present formulation aims at describing the cell-mediated enzymatic degradation of hydrogel by considering the hydrogels as a mixture of three phases: (a) a solid phase (denoted by superscript 's') made of a cross-linked network of polymer chains, (b) a fluid phase (denoted by superscript 'f') that mainly consists of water and (c) a dissolved enzyme phase (denoted by superscript 'e'). The motion and evolution of such a medium are dictated by general balances, laws (mass and momentum balance) as well as constitutive relations. Before discussing these aspects, it is important to introduce relevant definitions and notations (Table 1) and discuss a few assumptions aimed at simplifying the overall analysis. Let us consider a material point (belonging to the gel) of which the position is described by the vector $\mathbf{x}$ in a fixed cartesian coordinate system. Consistent with continuum mixture theory, such a material point represents a 'particle' made of the three interpenetrating phases with respective volume fraction $\phi^\alpha(\mathbf{x})$, where the index $\alpha = \mathrm{s}, \mathrm{f}, \mathrm{e}$ represents each particular phase. With this definition, it is possible to define an effective density $\rho^\alpha(\mathbf{x})$ that represents the mass of constituent $\alpha$ per total mixture volume. In other words, $\rho^\alpha$ is related to the real density $\rho_R^\alpha$ of constituent $\alpha$ by

$$\rho^\alpha(\mathbf{x}) = \rho_R^\alpha \phi^\alpha(\mathbf{x}). \tag{1}$$

Table 1. Notation definitions.

| Symbols | Definitions |
|---|---|
| $p$ | Fluid pressure |
| $\mathbf{T}^{\mathrm{e}}$ | Effective stress |
| $c$ | Concentration of enzyme |
| $\kappa$ | Permeability of water |
| $\tilde{\mu_f}$ | Viscosity of water |
| $\phi^{\mathrm{f}}$ | Volume fraction of fluid |
| $\mathbf{J}_w$ | Flux of water |
| $\mathbf{J}_{\mathrm{e}}$ | Flux of enzyme |
| $D$ | Diffusion coefficient of solute in pure solvent |
| $r_{\mathrm{s}}$ | Hydrodynamic radius of the solute |
| $\xi$ | Mesh size of hydrogel matrix |
| $\mu$ | Shear modulus |
| $\lambda$ | Lamè's first parameter |
| $M_c$ | Molecular weight between cross-links |
| $M_n$ | Molecular weight of linear chains |
| $M_r$ | Molecular weight of repeat unit of polymer backbone |
| $M_{\mathrm{e}}$ | Molecular weight of the enzyme |
| $\rho$ | Density of polymer |
| $\bar{v}$ | Specific volume of the polymer |
| $\rho_x$ | Cross-linking density |
| $\rho_{x0}$ | Initial cross-linking density |
| $V_\alpha$ | Volume of constituent $\alpha$ |
| $m_\alpha$ | Mass of constituent $\alpha$ |
| $\Omega$ | Rate of reaction of cross-link degradation |
| $\mathbf{v}^\alpha$ | True velocity of constituent $\alpha$ |
| $\mathbf{v}_{\mathrm{s}}^\alpha$ | Superficial velocity of constituent $\alpha$ relative to the solid velocity |
| $l$ | Bond length of polymer repeat unit |
| $k_2$ | Michaelis–Menten catalytic reaction rate of the enzyme |
| $K_m$ | Michaelis–Menten constant |
| $C_n$ | Flory characteristic ratio |
| $\chi$ | Flory polymer–solute interaction parameter |
| $p_{\mathrm{osm}}$ | Osmotic pressure |

At this point, the following three assumptions can be made regarding the hydrogel systems considered in this study:

(1) Enzyme is present in very small amounts relative to the volume of the fluid and solid phases, such that its volume fraction $\phi^{\mathrm{e}}$ can be neglected. In other words, we can write

$$\phi^{\mathrm{e}} \ll \phi^{\mathrm{s}} \quad \text{and} \quad \phi^{\mathrm{e}} \ll \phi^{\mathrm{f}}. \tag{2}$$

(2) The hydrogel consists only of solid, fluid and enzyme phases. This means that the summation of the volume fraction of each phase should equal unity. Neglecting the contribution of the enzyme phase by considering assumption (1), we can thus write

$$\phi^{\mathrm{f}} + \phi^{\mathrm{s}} = 1 \tag{3}$$

(3) As the hydrogels are subjected to low pressures, it is reasonable to consider that all constituents are incompressible. In other words, the real density $\rho_R^\alpha$ of each phase remains constant in space and time.

The above assumptions were applied to the balance of mass and momentum within the hydrogel to obtain the governing equations of the hydrogel system.

### *2.1 Mass conservation*

In the present study, it is assumed that degradation results in cleavage of polymer cross-links but does not affect its mass. This assumption is reasonable during the early stages of degradation. In this context, the mass of each mixture constituent is conserved during degradation and one can write

$$\frac{\partial \rho^\alpha}{\partial t} + \nabla\cdot(\rho^\alpha \mathbf{v}^\alpha) = 0 \quad \alpha = \mathrm{s}, \mathrm{f}, \mathrm{e}, \tag{4}$$

where $\mathbf{v}^\alpha$ represents the velocity of constituent $\alpha$ in a fixed cartesian coordinate system, $\nabla$ is the spatial differential operator and the operation '$\cdot$' denotes the scalar product. To simplify the formulation, it is common to rewrite the equation in terms of relative motion with respect to the solid skeleton. Doing so enables us to consider a Lagrangian formulation for solid deformation and an Eulerian type approach to treat water and enzyme transport. Rewriting the solid velocity as $\mathbf{v} = \mathbf{v}^{\mathrm{s}}$, one can show that the balance of mass for each constituent takes the form

$$\dot{\phi}^{\mathrm{s}} + \phi^{\mathrm{s}}\nabla\cdot\mathbf{v} = 0, \tag{5}$$

$$\dot{\phi}^{\mathrm{f}} + \nabla\cdot\mathbf{J}^{\mathrm{f}} + \phi^{\mathrm{f}}\nabla\cdot\mathbf{v} = 0, \tag{6}$$

$$\dot{\phi}^{\mathrm{e}} + \nabla\cdot\mathbf{J}^{\mathrm{e}} + \phi^{\mathrm{e}}\nabla\cdot\mathbf{v} = 0, \tag{7}$$

where the superimposed dot represents the material time derivative D/D$t$ of a field associated with solid motion, that is

$$\dot{a} = \frac{\mathrm{D}a}{\mathrm{D}t} = \frac{\partial a}{\partial t} + \mathbf{v}\cdot\nabla a, \tag{8}$$

for any $a(\mathbf{x}, \mathbf{t})$ that are smooth functions of space and time. Furthermore, we introduced the relative flux $\mathbf{J}^{\mathrm{f}}$ and $\mathbf{J}^{\mathrm{e}}$ of water and enzyme, respectively, as

$$\mathbf{J}^{\mathrm{f}} = \phi^{\alpha}(\mathbf{v}^{\alpha} - \mathbf{v}) \quad \alpha = \mathrm{f}, \mathrm{e}. \tag{9}$$

Using assumption (3), one can rewrite the mass balance in a simpler form as follows:

$$\dot{\phi}^{\mathrm{f}} = (1 - \phi^{\mathrm{f}})\nabla\cdot\mathbf{v}, \tag{10}$$

$$\nabla\cdot\mathbf{J}^{\mathrm{f}} = -\nabla\cdot\mathbf{v}, \tag{11}$$

$$\dot{\phi}^{\mathrm{e}} + \nabla\cdot\mathbf{J}^{\mathrm{e}} = -\phi^{\mathrm{e}}\nabla\cdot\mathbf{v}, \tag{12}$$

where the first equation characterises the change in water volume fraction $\phi^{\mathrm{f}}$ with volumetric gel deformation $\nabla\cdot\mathbf{v}$. The second equation is the mass balance of the fluid–solid mixture, obtained by summing (5) and (6), and the third equation is the conservation of enzyme mass.

### 2.2 Balance of momentum

In the absence of external body forces and neglecting the effect of inertia for the slow process of degradation, the balance of momentum for each phase is commonly written in terms of the partial Cauchy stress $\mathbf{T}^{\alpha}$ associated with constituent $\alpha$ as follows:

$$\nabla\cdot\mathbf{T}^{\alpha} + \mathbf{f}^{\alpha} = 0 \quad \alpha = \mathrm{s}, \mathrm{f}, \mathrm{e}. \tag{13}$$

In the above equation, $\mathbf{f}^{\alpha}$ is the resultant body force exerted by the other constituents on constituent $\alpha$. Internal equilibrium of the mixture implies that the summation of these forces should globally vanish, i.e. $\mathbf{f}^{\mathrm{s}} + \mathbf{f}^{\mathrm{f}} + \mathbf{f}^{\mathrm{e}} = 0$. Invoking the effective stress principle and assuming the fluid is inviscid for the slow fluid velocities in the gel, the partial solid and fluid stresses are written in terms of fluid pressure $p$ in the form

$$\mathbf{T}^{\mathrm{s}} = \mathbf{T}^{\mathrm{se}} - \phi^{\mathrm{s}}p\mathbf{I} \quad \text{and} \quad \mathbf{T}^{\mathrm{f}} = -\phi^{\mathrm{f}}p\mathbf{I}, \tag{14}$$

where $\mathbf{T}^{\mathrm{se}}$ is the effective solid stress, $\mathbf{I}$ is the second order identity tensor and the fluid pressure is positive in compression. In addition, using the fact that the enzyme volume fraction is small compared with those of fluid and solid, are the contribution of the enzyme's partial stress $\mathbf{T}^{\mathrm{e}}$. Thus, considering (13) and (14), neglected we can write the balance of momentum for the entire mixture in the form

$$\nabla\cdot\mathbf{T} = 0, \quad \text{where } \mathbf{T} = \mathbf{T}^{\mathrm{s}} + \mathbf{T}^{\mathrm{f}} = \mathbf{T}^{\mathrm{se}} - p\mathbf{I}. \tag{15}$$

Here, $\mathbf{T}$ is the Cauchy stress of the mixture, which satisfies the symmetry requirements imposed by the balance of angular momentum ($\mathbf{T} = \mathbf{T}^{T}$).

### 2.3 Centro-symmetric formulation

Limiting our analysis to 3D hydrogels with low cell density, the problem can be simplified to a single enzyme-producing spherical cell of radius $R_c$, located in the centre of a hydrogel sphere of radius $R_g$. On the basis of symmetry arguments, it can easily be shown that in this case, solid displacement, water and enzyme flow occur in a radial direction from the centre of the cell. This observation allows us to simplify the original 3D problem into a 1D 'centro-symmetric' problem for which the various physical fields can be expressed in terms of time $t$ and their distance $r$ from the centre of the cell (Figure 1). In particular, at any time $t$, we are looking for a solution in terms of three variables,

$$u(r,t), \quad p(r,t), \quad \text{and} \quad c(r,t), \tag{16}$$

representing the radial displacement of the solid, the pressure of water and the concentration of enzyme, respectively. These functions are determined by solving a system of three coupled differential equations, composed of the mass balance of the fluid–solid mixture (11) and the enzyme (12), together with the momentum balance equation (13). Under centro-symmetric assumptions, one can show that (11), (12) and (15) take the form

$$\frac{1}{r^2}\frac{\partial}{\partial r}(r^2\mathrm{J}^{\mathrm{f}}) + \frac{1}{r^2}\frac{\partial}{\partial r}(r^2\dot{u}) = 0, \tag{17}$$

$$\frac{\partial}{\partial t}(\phi^{\mathrm{f}}c) + \frac{1}{r^2}\frac{\partial}{\partial r}(r^2\mathrm{J}^{\mathrm{e}}) + \frac{1}{r^2}\frac{\partial}{\partial r}(r^2\phi^{\mathrm{f}}c\dot{u}) = 0, \tag{18}$$

$$\frac{\partial \mathrm{T}^{\mathrm{se}}_{rr}}{\partial r} + \frac{1}{r}(2\mathrm{T}^{\mathrm{se}}_{rr} - \mathrm{T}^{\mathrm{se}}_{\theta\theta} - \mathrm{T}^{\mathrm{se}}_{\phi\phi}) - \frac{1}{3}\frac{\partial p}{\partial r} = 0, \tag{19}$$

where $\mathrm{J}^{\mathrm{f}}$ and $\mathrm{J}^{\mathrm{e}}$ are the water and enzyme relative flux in the radial directions and $\mathrm{T}^{\mathrm{se}}_{rr}$, $\mathrm{T}^{\mathrm{se}}_{\theta\theta}$ and $\mathrm{T}^{\mathrm{se}}_{\phi\phi}$ are components of the Cauchy stress tensor in the radial and circumferential directions, respectively. The above time-dependent

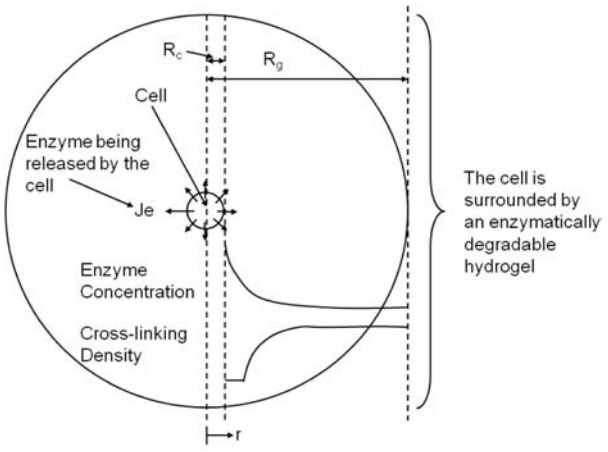


Figure 1. Diagram of centro-symmetric cell-mediated gel degradation problem. A spherical cell (in the centre) isotropically releases an enzyme in an enzymatically degradable hydrogel.

boundary value problem can be solved upon the knowledge of initial conditions (at time $t = 0$):

$$u(r,0) = 0 \;\; p(r,0) = p_{\text{osm}} \;\; c(r,0) = 0, \tag{20}$$

where $p_{\text{osm}}$ is the osmotic pressure in the gel. In addition, a set of boundary conditions must be applied for each fields at $r = R_c$ and at $r = R_{\text{g}}$. In terms of solid displacement, it is assumed that the cell boundary does not move during degradation and thus $u(R_c, t) = 0$, while the gel is assumed to be in a global stress free state. The latter assumption can be written in terms of a vanishing radial stress $\text{T}^{\text{se}}_{rr}$ on the gel boundary. Boundary conditions related to the fluid are based on the fact that there is no water flux on the cell boundary ($\text{J}^{\text{f}}(R_c, t) = 0$) but water may flow out of the gel at $R = R_{\text{g}}$ (i.e. $p = p_{\text{osm}}$, the osmotic pressure). To quantify the enzyme production by the cell, we assume that the cell produces a constant flux $\text{J}^{\text{e}}_0$ at its outer membrane, which leads to the condition $\text{J}^{\text{e}}(R_c, t) = \text{J}^{\text{e}}_0$. This assumption is realistic if the cell actively produces the enzyme, regardless of its external concentration. Finally, assuming that the hydrogel domain is surrounded by a fluid that allows fast enzyme diffusion, it is acceptable to assume that enzyme concentration is negligible at the outer surface of the hydrogel ($c = 0$ at $r = R_{\text{g}}$). A summary of the boundary conditions is given in Table 2.

## 3. Constitutive equations

To complete the model, this section introduces the constitutive relation to describe the interactions between degradation, gel deformation and fluid–enzyme transport. We start by introducing a rubber elasticity formulation to characterise the mechanical response of the gel.

### *3.1 Mechanical response of the gel: rubber elasticity and equilibrium swelling theories*

In the context of small strain, linear elasticity theory, the relationship between the effective stress $\mathbf{T}^{\text{se}}$ and strain $\mathbf{E} = 1/2\big((\nabla \mathbf{u}) + (\nabla \mathbf{u})^T\big)$ is given in terms of the elasticity tensor $\mathbf{C}$. Assuming an isotropic gel, tensor $\mathbf{C}$ can by expressed in a matrix form in terms of the shear modulus $\mu$ and Lamé's first parameter $\lambda$:

$$\begin{bmatrix} \text{T}^{\text{se}}_{rr} \\ \text{T}^{\text{se}}_{\theta\theta} \\ \text{T}^{\text{se}}_{\phi\phi} \end{bmatrix} = \begin{bmatrix} 2\mu+\lambda & \lambda & \lambda \\ \lambda & 2\mu+\lambda & \lambda \\ \lambda & \lambda & 2\mu+\lambda \end{bmatrix} \begin{bmatrix} \frac{\partial u_r}{\partial r} \\ \frac{u_r}{r} \\ \frac{u_r}{r} \end{bmatrix}, \tag{21}$$

where we only considered the non-zero component of the strain tensor in centro-symmetric assumptions. Furthermore, Lamé's first parameter can be related to the shear modulus and Poisson's ratio:

$$\lambda = \frac{2\mu\nu}{1-2\nu}, \tag{22}$$

where the Poisson ratio $\nu \approx 0.5$ for a nearly incompressible material as considered in this study (a value of $\nu = 0.49$ is used for simulation). With these assumptions, the degradation of the gel is characterised by the change in shear modulus $\mu$ with cross-link density. The two predominate theories used to elucidate the structure of the hydrogel are the equilibrium swelling theory and the rubber elasticity theory. For non-ionic hydrogels, Flory–Rehner theory, which encompasses both theories, has been used to predict the hydrogel structure and specifically the average molecular weight $\bar{M}_c$ of the polymer chain between two neighbouring cross-links. In this model, the relation between $\bar{M}_c$ and the average molecular weight $\bar{M}_n$ of the polymer chains cross-linking is given by Bell and Peppas (1995), Peppas and Barr-Howell (1986)

$$\frac{1}{\bar{M}_c} = \frac{2}{\bar{M}_n} - \frac{\bar{\nu}\big[\ln(1-n_{\text{s}}) + n_{\text{s}} + \chi_1 n_{\text{s}}^2\big]}{V_1\left(n_{\text{s}}^{1/3} - \frac{n_{\text{s}}}{2}\right)}, \tag{23}$$

where $\bar{\nu}$ is the specific volume of the polymer, $V_1$ is the molar volume of water, $n_{\text{s}}$ is the polymer volume fraction in the swollen state and $\chi_1$ is the polymer–solvent interaction parameter. From experimental measurements of $n_{\text{s}}$, the average molecular weight between cross-links can be determined. Furthermore, when taken in their swollen state and subjected to small deformations, hydrogels are known to exhibit rubbery-like elastic behaviours (Anseth et al. 1996). As a consequence, from knowledge of the hydrogel structure as determined from the Flory–Rehner theory above, the shear modulus can be predicted from the rubber elasticity theory by

$$\mu = \frac{\rho R T}{\bar{M}_c}\frac{r_0^2}{r_{\text{f}}^2}\left(1 - \frac{2\bar{M}_c}{\bar{M}_n}\right), \tag{24}$$

where $\rho$ is the polymer density, $R$ is the universal gas constant, $T$ is the absolute experimental temperature, $r_0^2/r_{\text{f}}^2$ is the ratio of the end-to-end distance in a real network to the end-to-end network of isolated chains. Typically, this ratio is close to unity for hydrogels systems (Anseth et al. 1996), i.e. we consider $r_0^2/r_{\text{f}}^2 = 1$ in this study. As

Table 2. Summary of boundary conditions.

| | Solid | | Water | | Enzyme | |
|---|---|---|---|---|---|---|
| | Neumann | Dirichlet | Neumann | Dirichlet | Neumann | Dirichlet |
| $r = R_c$ | | $u = 0$ | $\text{J}^{\text{f}} = 0$ | | $\text{J}^{\text{e}} = \text{J}^{\text{e}}_0$ | |
| $r = R_g$ | $\text{T}^{\text{se}}_{rr} = 0$ | | | $p = p_{\text{osm}}$ | | $c = 0$ |

hydrogels experience a significant amount of swelling due to their hydrophilic nature, another important parameter is their swelling pressure. This swelling pressure $p$ develops through contributions from the elastic pressures, $\hat{p}$, exerted by the cross-links on the hydrogel network and the osmotic pressure, $p_{\text{osm}}$, which arises due to mixing of the polymer chains and the water molecules. The swelling pressure is, therefore, defined by Horkay et al. (2000)

$$p = \hat{p} + p_{\text{osm}}, \tag{25}$$

where $\hat{p}$ is related to the shear modulus through the rubber elasticity theory and $p_{\text{osm}}$ is described by the Flory–Huggins theory as follows, Flory (1941):

$$\hat{p} = -\mu, \tag{26}$$

$$p_{\text{osm}} = -\frac{RT}{V_1}\left[\ln(1 - n_{\text{s}} + n_{\text{s}} + \chi_1 n_{\text{s}}^2)\right]. \tag{27}$$

Changes in the network structure due to degradation can be described by two parameters; the cross-linking density, $\rho_x$, and the correlation length or mesh size, $\xi$. The cross-linking density (mol $\text{l}^{-1}$) can be determined in terms of $M_c$ by

$$\rho_x = \frac{1}{\bar{v}\bar{M}_c}, \tag{28}$$

whereas the mesh size is generally defined as the average distance between two adjacent cross-links and in essence describes the size of the pores within the hydrogel. Peppas and Barr-Howell (1986) and Bell and Peppas (1995) have shown that $\xi$ can be written in terms of the average length $\ell$ of a bond (nm) in the polymer backbone and the number $n$ of bonds between cross-links as

$$\xi = n_{\text{s}}^{-1/3}(C_n n)^{1/2}\ell, \tag{29}$$

where $C_n$ is the Flory characteristic ratio for the polymer.

### 3.2 Degradation kinetics

The degradation kinetics of enzymatically susceptible hydrogels have been shown to follow Michaelis–Menton kinetics (Lutolf et al. 2003; Levesque and Shoichet 2007). For the case in which the peptide sequence is located within the cross-links of the hydrogel, the concentration of the peptide (i.e. substrate for the enzyme) is simply defined by the cross-linking density. Therefore, the rate equation following Michaelis–Menton analysis is defined as a function of cross-linking density and enzyme concentration $c$ by

$$\frac{\partial \rho_x}{\partial t} = -\frac{k_2 c \rho_x}{K_m + \rho_x}, \tag{30}$$

where $k_2$ ($\text{s}^{-1}$) (often defined as $k_{\text{cat}}$) and $K_m(M)$ are the Michaelis–Menton kinetic constants. In this form, the rate equation will change with degradation as cross-links are cleaved. A unique characteristic of the degradation behaviour of hydrogels is the fact that when there are fewer than two cross-links per polymer chain, the hydrogel transitions from a cross-linked polymer to highly branched, but soluble polymer chains. This point is referred to as the reverse gelation point. For simplicity, this model describes the degradation behaviour of the hydrogel under conditions for which reverse gelation has not yet been reached. As such, the limit of hydrogel degradation has been set to occur at the point at which 60% of the cross-links have been degraded. Reverse gelation has been shown to occur when 60%–80% of the hydrogel mass has been lost (Metters et al. 2000; Martens and Anseth 2000). Therefore, for highly swollen and loosely cross-linked hydrogels, which are often employed in tissue engineering applications, the point at which 60% of the cross-links have been degraded reasonably represents a highly degraded, but not soluble, region of the hydrogel.

### 3.3 Fluid and enzyme transport

Let us finally introduce the constitutive relations for the relative fluxes $\mathbf{J}^{\text{f}}$ and $\mathbf{J}^{\text{e}}$ of fluid and enzyme, respectively. Considering the hydrogel as a dense isotropic porous medium, we can describe the fluid flux by Darcy's law in terms of the pressure gradient $\nabla p$ as

$$\mathbf{J}^{\text{f}} = -\kappa \nabla p. \tag{31}$$

The gel's isotropic permeability, represented by the scalar $\kappa$ can be related to the average polymer mesh size $\xi$ by Holmes and Mow (1990)

$$\kappa = \frac{\xi^2 \phi^{\text{f}}}{8\tilde{\mu}_{\text{f}}\delta}, \tag{32}$$

where $\delta$ is the tortuosity and $\tilde{\mu}_{\text{f}}$ is the fluid viscosity. To derive an expression for the enzyme flux, it is of interest to decompose $\mathbf{J}^{\text{e}}$ into a component following the water motion and a term related to the diffusion of enzyme within water,

$$\mathbf{J}^{\text{e}} = \phi^{\text{e}}\left(\mathbf{v}^{\text{e}} - \mathbf{v}^{\text{f}}\right) + \phi^{\text{e}}\left(\mathbf{v}^{\text{f}} - \mathbf{v}\right). \tag{33}$$

Using the fact that the first term is related to enzyme diffusion within water, which can be described by Fick's law of diffusion as follows:

$$c(\mathbf{v}^{\text{e}} - \mathbf{v}^{\text{f}}) = -D_{\text{g}}\nabla c, \tag{34}$$

where $D_{\text{g}}$ is the diffusion constant of the enzyme within the hydrogel and recognising that the second term is related to water flux by

$$\phi^{\text{e}}\left(\mathbf{v}^{\text{f}} - \mathbf{v}\right) = \frac{\phi^{\text{e}}}{\phi^{\text{f}}}\mathbf{J}^{\text{f}}, \tag{35}$$

we thus obtain the following expression for the flux of enzyme through the gel:

$$\mathbf{J}^{\text{e}} = -\frac{\phi^{\text{f}} M^{\text{e}}}{\rho_R^{\text{e}}} D_{\text{g}}\nabla c - \frac{M^{\text{e}} c}{\rho_R^{\text{e}}}\kappa \nabla p. \tag{36}$$

Note that to derive the above equation, we used the fact that $\phi^{\mathrm{e}} = \phi^{\mathrm{f}} M^{\mathrm{e}} c/\rho_R^{\mathrm{e}}$. Diffusion of the enzyme through the hydrogel is strongly dependent on the ratio between the hydrogel mesh size and the enzyme effective radius $r_{\mathrm{s}}$ as well as the degree of gel swelling. Lustig and Peppas (1988) have developed a model to describe the effective diffusivity of a solute diffusing through a cross-linked hydrogel using a free volume approach. They proposed the following relation:

$$D_{\mathrm{g}} = D_\infty \left(1 - \frac{r_{\mathrm{s}}}{\xi}\right) \exp\left(-Y \frac{\phi^{\mathrm{s}}}{1-\phi^{\mathrm{s}}}\right), \tag{37}$$

where $D_\infty$ is the diffusion coefficient of the solute in pure solvent and $Y$ is a correction factor that represents critical volume required for the solute to undergo a successful translational movement relative to the average free volume per molecule of the solvent, which can be approximated as unity. The quantity $D_\infty$ can be approximated by the Stokes–Einstein equation,

$$D_\infty = \frac{k_b T}{6\pi \tilde{\mu}_{\mathrm{f}} r_{\mathrm{s}}}, \tag{38}$$

where $k_b$ is the Boltzman constant, $r_{\mathrm{s}}$ is the Stokes–Einstein hydrodynamic radius of the solute, $T$ is the absolute temperature and $\tilde{\mu}_{\mathrm{f}}$ is the viscosity of the solvent.

## 4. Finite element formulation

To investigate the dynamics of enzymatic degradation of hydrogel, one needs to obtain a solution of governing Equations (17)–(19), together with the constitutive relations. This leads to a highly nonlinear system of coupled PDEs for which the determination of a closed-form solution is challenging. These difficulties maybe avoided by seeking a numerical solution of the equations using the finite element method (FEM). This section describes the procedure to convert the original system of PDEs into a system of algebraic equations corresponding to an equivalent discretised system. Following standard FEM procedures (Chandrupatla and Belegundu 2002), we present a description of three characteristic steps to derive the FEM equations: (a) conversion from the strong form to the weak form of the system of PDE, (b) spatial discretisation of the system into finite elements and (c) time discretisation and integration.

### *4.1 Weak form of the governing equations*

Using the standard Galerkin weighted method, we multiplied the governing equations (17)–(19) by arbitrary weighting functions $w(r)$, $x(r)$ and $y(r)$ which relate to $u$, $p$ and $c$, respectively, and integrated over the entire domain ($R_{\mathrm{c}} \le r \le R_{\mathrm{g}}$). These equations are then expanded by applying the divergence theorem that allows us to consider the boundary conditions. In particular, the weighting functions vanish on boundaries for which the Dirichlet boundary conditions are applied on the corresponding fields. For our particular formulation, this yields

$$w(R_{\mathrm{c}}) = x(R_{\mathrm{g}}) = y(R_{\mathrm{g}}) = 0. \tag{39}$$

After applying the boundary conditions, we obtain the weak form of the governing equation in the following form:

$$\int_{R_{\mathrm{c}}}^{R_{\mathrm{g}}} \frac{\partial}{\partial r}(\dot{u}) x(r)\mathrm{d}r - \int_{R_{\mathrm{c}}}^{R_{\mathrm{g}}} \mathbf{J}_{\mathrm{f}} \frac{\partial x}{\partial r}\mathrm{d}r = 0, \tag{40}$$

$$\int_{R_{\mathrm{c}}}^{R_{\mathrm{g}}} \left( r^2 \frac{\partial \phi^{\mathrm{f}} c}{\partial t} y(r) - r^2 J_{\mathrm{e}} \frac{\partial y}{\partial r} + \frac{\partial}{\partial r}(r^2 \phi^{\mathrm{f}} c \dot{u}) y(r) \right) \mathrm{d}r = y(R_{\mathrm{c}}) \hat{J}_{\mathrm{e}0} R_{\mathrm{c}}^2, \tag{41}$$

$$\int_{R_{\mathrm{c}}}^{R_{\mathrm{g}}} \left( r^2 \mathbf{T}^{\mathrm{e}}_{rr} \frac{\partial w}{\partial r} + 2rw(r)\mathbf{T}^{\mathrm{e}}_{\theta\theta} \right) \mathrm{d}r - \frac{1}{3}\int_{R_{\mathrm{c}}}^{R_{\mathrm{g}}} \left( r^2 \bar{p} \frac{\partial w}{\partial r} + 2r\bar{p} w(r) \right) \mathrm{d}r = w(R_{\mathrm{g}}) R_{\mathrm{g}}^2 p_{\mathrm{osm}}. \tag{42}$$

This set of nonlinear equations is typically solved with an iterative solver (such as the Newton–Raphson method). For this reason, a linearisation of the above equations is necessary. This is done by taking a Taylor approximation of each variable (denoted by $f$ for convenience) in terms of a 'constant' term $\tilde{f}$ and small variation $\delta f$, such that $f \approx \tilde{f} + \delta f$. Only considering first order terms, the linearised weak form equations can be written as:

$$\int_{R_{\mathrm{c}}}^{R_{\mathrm{g}}} [\,1 \quad 1\,] \begin{bmatrix} r^2 \frac{\partial}{\partial r}(\dot{u}) \\ 2r\dot{u} \end{bmatrix} x(r)\mathrm{d}r + \frac{A^2 \phi^{\mathrm{f}}}{H} \int_{R_{\mathrm{c}}}^{R_{\mathrm{g}}} \left( \frac{1}{\tilde{\rho}_x} \frac{\partial \delta\bar{p}}{\partial r} - \frac{1}{\tilde{\rho}_x^2} \delta\rho_x \frac{\partial \tilde{\bar{p}}}{\partial r} + \frac{1}{\tilde{\rho}_x} \frac{\partial \tilde{\bar{p}}}{\partial r} \right) \frac{\partial x}{\partial r} r^2 \mathrm{d}r = 0 \tag{43}$$

$$\int_{R_{\mathrm{c}}}^{R_{\mathrm{g}}} r^2 \phi^{\mathrm{f}} \dot{c} y(r) + \Bigg( (1-\phi^{\mathrm{f}}) \tilde{c} [1 \quad 1]. + \left[ \phi^{\mathrm{f}} \tilde{c}, \phi^{\mathrm{f}} \tilde{c} + \frac{r}{2}\tilde{c}\frac{\partial \phi^{\mathrm{f}}}{\partial r} + \frac{r}{2}\phi^{\mathrm{f}} \frac{\partial \tilde{c}}{\partial r} \right] \Bigg) \begin{bmatrix} r^2 \frac{\partial \dot{u}}{\partial r} \\ 2r\dot{u} \end{bmatrix} y(r) + r^2 \left[ \tilde{c} \frac{A^2 \phi^{\mathrm{f}}}{H\tilde{\rho}_x} \frac{\partial \delta\bar{p}}{\partial r} + \frac{A^2 \phi^{\mathrm{f}}}{H\tilde{\rho}_x} \frac{\partial \tilde{\bar{p}}}{\partial r} \right]$$
$$\delta c + \phi^{\mathrm{f}} D (1 - \hat{\psi} \frac{r_h \tilde{\rho}_x^{1/2}}{A}) \frac{\partial \delta c}{\partial r} + \left( -\frac{1}{2}\phi^{\mathrm{f}} D \hat{\psi} \frac{r_h}{A\tilde{\rho}_x^{1/2}} \frac{\partial \tilde{c}}{\partial r} - \tilde{c} \frac{A^2 \phi^{\mathrm{f}}}{H\tilde{\rho}_x^2} \frac{\partial \tilde{\bar{p}}}{\partial r} \right) \delta\rho_x + \phi^{\mathrm{f}} D (1 - \hat{\psi} \frac{r_h \tilde{\rho}_x^{1/2}}{A}) \frac{\partial \tilde{c}}{\partial r} + \tilde{c} \frac{A^2 \phi^{\mathrm{f}}}{H\tilde{\rho}_x} \frac{\partial \tilde{\bar{p}}}{\partial r} \Bigg] \frac{\partial y}{\partial r} \mathrm{d}r = y(r) \hat{J}_{\mathrm{e}0} R_{\mathrm{c}}^2, \tag{44}$$

$$
\begin{aligned}
RT\int_{R_c}^{R_g}\left(\tilde{\rho}_x-\rho_p\frac{2}{\bar{M}_n}\right)\frac{1}{r^2}\begin{bmatrix} r^2\frac{\partial w}{\partial r} & 2rw(r)\end{bmatrix}\hat{\mathbf{C}}\begin{bmatrix} r^2\frac{\partial}{\partial r}(\delta u)\\ 2r\delta u\end{bmatrix}\\
+\frac{1}{r^2}\begin{bmatrix} r^2\frac{\partial w}{\partial r} & 2rw(r)\end{bmatrix}\hat{\mathbf{C}}\begin{bmatrix} r^2\frac{\partial}{\partial r}(\tilde{u})\\ 2r\tilde{u}\end{bmatrix}\delta\rho_x\,\mathrm{d}r\\
+RT\int_{R_c}^{R_g}\left(\tilde{\rho}_x-\rho_p\frac{2}{\bar{M}_n}\right)\frac{1}{r^2}\begin{bmatrix} r^2\frac{\partial w}{\partial r} & 2rw(r)\end{bmatrix}\hat{\mathbf{C}}\begin{bmatrix} r^2\frac{\partial}{\partial r}(\tilde{u})\\ 2r\tilde{u}\end{bmatrix}\mathrm{d}r\\
-\frac{1}{3}\int_{R_c}^{R_g}\begin{bmatrix} r^2\frac{\partial w}{\partial r} & 2rw(r)\end{bmatrix}\begin{bmatrix}1\\1\end{bmatrix}p_f\,\mathrm{d}r\\
-\frac{1}{3}\int_{R_c}^{R_g}\begin{bmatrix} r^2\frac{\partial w}{\partial r} & 2rw(r)\end{bmatrix}\begin{bmatrix}1\\1\end{bmatrix}\delta p_f\,\mathrm{d}r=w(r)R_g^2p_{osm},
\end{aligned}
\tag{45}
$$

where the matrix $\hat{\mathbf{C}}$ is introduced as

$$
\hat{\mathbf{C}}=\begin{bmatrix}\left(2+\frac{2\nu}{1-2\nu}\right) & \frac{2\nu}{1-2\nu}\\ \frac{2\nu}{1-2\nu} & \left(1+\frac{2\nu}{1-2\nu}\right)\end{bmatrix}. \tag{46}
$$

### 4.2 Discretisation

Proceeding to the finite element dicretisation, the hydrogel domain is subdivided in $n_e$ elements of length $\ell_e$. In this work, a mixed finite element formulation is used, based on linear, two-point, Lagrange interpolation functions to approximate pressure $p$, enzyme concentration $c$ and quadratic, three-point, Lagrange interpolation functions to approximate the displacement field $u$. The solution fields in an element e are then represented by a vector $\mathbf{d}^e$ as follows:

$$
\mathbf{d}^e=\begin{Bmatrix}u_1^e & p_1^e & c_1^e & u_2^e & p_2^e & c_2^e & u_3^e\end{Bmatrix}^T, \tag{47}
$$

where the subscripts represent the number of the nodes (1,2 or 3) associated with element e. The interpolations of solution fields within an element are then written in terms of linear and quadratic shape functions (represented by vectors $\mathbf{N}$ and $\mathbf{M}$, respectively), such that

$$
\begin{aligned}
&p_h^e(r)=\sum_{I=1}^{2}\mathbf{N}^I(r)p_I^e,\quad c_h^e(r)=\sum_{I=1}^{2}\mathbf{N}^I(r)c_I^e\quad\text{and}\\
&u_h^e(r)=\sum_{I=1}^{3}\mathbf{M}^I(r)u_I^e,
\end{aligned}
\tag{48}
$$

where $p_h^e(r)$, $c_h^e(r)$ and $u_h^e(r)$ are the numerical approximation of the solution fields in element e. In addition, the shape function $\mathbf{N}^I$ and $\mathbf{M}^I$ are the standard linear and quadratic shape functions associated with node $I$ (Chandrupatla and Belegundu 2002). Discretising the weak forms (43)–(45) by splitting the integral into a summation of integrals over elements and substituting the solution fields and weighting functions by their interpolated form (48), one obtains global system of ordinary differential equations with respect to time,

$$
\mathbf{C}\cdot\mathbf{d}+\mathbf{K}\cdot\delta\mathbf{d}+\mathbf{b}_n=0, \tag{49}
$$

where the global solution vector $\mathbf{d}$ results from the assembly of the individual element vector $\mathbf{d}^e$. Similarly, the damping and stiffness matrices $\mathbf{C}$ and $\mathbf{K}$, respectively, as well as the vector $\mathbf{b}_n$ result of the assembly operation relating element to global degrees of freedom. If we denote by $A$ the assembly operation, we have

$$
\mathbf{C}=A(\mathbf{C}^e),\quad \mathbf{K}=A(\mathbf{K}^e)\quad\text{and}\quad \mathbf{b}_n=A\left(\mathbf{b}_n^e\right), \tag{50}
$$

where the element damping, stiffness matrices and $b_n$ vector have the following forms:

$$
\begin{aligned}
\mathbf{C}^e&=\begin{bmatrix}0 & 0 & 0\\ \mathbf{C}_{2u}^e & 0 & 0\\ \mathbf{C}_{3u}^e & 0 & \mathbf{C}_{3e}^e\end{bmatrix},\\
\mathbf{K}^e&=\begin{bmatrix}\mathbf{K}_{1u}^e & \mathbf{K}_{1p}^e & 0\\ 0 & \mathbf{K}_{2p}^e & 0\\ 0 & \mathbf{K}_{3p}^e & \mathbf{K}_{3e}^e\end{bmatrix}\quad\text{and}\quad \mathbf{b}^e=\begin{bmatrix}\mathbf{b}_1^e\\ \mathbf{b}_2^e\\ \mathbf{b}_3^e\end{bmatrix}.
\end{aligned}
\tag{51}
$$

After a tedious but straightforward derivation, one can show that the element sub-matrices appearing in the above expressions are written as

$$
\mathbf{C}_{2u}^e=\frac{\ell_e}{2}\int_{-1}^{1}\mathbf{N}^T\begin{bmatrix}1 & 1\end{bmatrix}\mathbf{B}_2\mathrm{d}\xi, \tag{52}
$$

$$
\begin{aligned}
\mathbf{C}_{3u}^e=&\frac{\ell_e}{2}\int_{-1}^{1}\mathbf{N}^T(1-\mathbf{N}(\phi^f)^e)\mathbf{N}c^e\begin{bmatrix}1 & 1\end{bmatrix}\mathrm{d}\xi\\
&+\frac{\ell_e}{2}\int_{-1}^{1}\Bigg[\mathbf{N}(\phi^f)^e\mathbf{N}c^e,\quad \mathbf{N}(\phi^f)^e\mathbf{N}c^e.\\
&+\frac{1}{2}\mathbf{N}r_e\mathbf{N}c^e\frac{\partial\phi^f}{\partial r}+\frac{1}{2}\phi^f\mathbf{B}_1c^e\Bigg)\mathbf{B}_2\,\mathrm{d}\xi,
\end{aligned}
\tag{53}
$$

$$
\mathbf{C}_{3e}^e=\frac{\ell_e}{2}\int_{-1}^{1}\mathbf{N}^T(\mathbf{N}r_e)^2\mathbf{N}(\phi^f)^e\mathbf{N}\,\mathrm{d}\xi, \tag{54}
$$

$$
\begin{aligned}
\mathbf{K}_{1u}^e=&\frac{\mathrm{R}\mathrm{T}\ell_e}{2}\int_{-1}^{1}\mathbf{B}_2^T\left(\mathbf{N}\rho_x^e-\rho_p\frac{2}{\bar{M}_n}\right)\\
&\times\frac{1}{(\mathbf{N}r^e)^2}\hat{\mathbf{C}}\mathbf{B}_2\,\mathrm{d}\xi,
\end{aligned}
\tag{55}
$$

$$
\mathbf{K}_{1p}^e=-\frac{\ell_e}{6}\int_{-1}^{1}\mathbf{B}_2^T\begin{bmatrix}1\\1\end{bmatrix}\mathbf{N}\,\mathrm{d}\xi, \tag{56}
$$

$$
\mathbf{K}_{2p}^e=\frac{\ell_e}{2}\int_{-1}^{1}\mathbf{B}_1^T\frac{A^2\phi^f}{H}\frac{1}{\mathbf{N}\rho_x^e}\mathbf{B}_1\,\mathrm{d}\xi, \tag{57}
$$

$$\mathbf{K}^{\mathrm{e}}_{3p} = \frac{\ell_{\mathrm{e}}}{2}\int_{-1}^{1} \mathbf{B}_1^T \mathbf{N} c^{\mathrm{e}} \frac{A^2\phi^{\mathrm{f}}}{H\mathbf{N}\rho_x^{\mathrm{e}}}\mathbf{B}_1 \,\mathrm{d}\xi, \tag{58}$$

$$\mathbf{K}^{\mathrm{e}}_{3\mathrm{e}} = \frac{\ell_{\mathrm{e}}}{2}\int_{-1}^{1} \mathbf{B}_1^T \left(\frac{A^2\phi^{\mathrm{f}}}{H\mathbf{N}\rho_x^{\mathrm{e}}}\mathbf{B}_1 p^{\mathrm{e}}\mathbf{N} + \mathbf{N}(\phi^{\mathrm{f}})^{\mathrm{e}} D \times \left(1 - \hat{\psi}\frac{r_h}{A}(\mathbf{N}\rho_x^{\mathrm{e}})^{1/2}\right)\mathbf{B}_1\right) \mathrm{d}\xi, \tag{59}$$

$$\mathbf{b}^{\mathrm{e}}_1 = \frac{\ell_{\mathrm{e}}}{2}\int_{-1}^{1} \mathbf{B}_2^T \left(\mathrm{RT}\left(\mathbf{N}\rho_x^{\mathrm{e}} - \rho_p\frac{2}{\bar{M}_n}\right)\frac{1}{(\mathbf{N}r^{\mathrm{e}})^2}\hat{\mathbf{C}}\mathbf{B}_2 u^{\mathrm{e}} - \frac{1}{3}\begin{bmatrix}1\\1\end{bmatrix}\mathbf{N}p^{\mathrm{e}}\right) \mathrm{d}\xi, \tag{60}$$

$$\mathbf{b}^{\mathrm{e}}_2 = \frac{\ell_{\mathrm{e}}}{2}\int_{-1}^{1} \mathbf{B}_1^T \left(\frac{A^2\phi^{\mathrm{f}}}{H}\frac{1}{(\mathbf{N}\rho_x^{\mathrm{e}})}\mathbf{B}_1 p^{\mathrm{e}}\right) \mathrm{d}\xi, \tag{61}$$

$$\mathbf{b}^{\mathrm{e}}_3 = \frac{\ell_{\mathrm{e}}}{2}\int_{-1}^{1} \mathbf{B}_1^T \left(\mathbf{N}c^{\mathrm{e}}\frac{A^2\phi^{\mathrm{f}}}{H\mathbf{N}\rho_x^{\mathrm{e}}}\mathbf{B}_1 p^{\mathrm{e}} + \mathbf{N}(\phi^{\mathrm{f}})^{\mathrm{e}} D \times \left(1 - \hat{\psi}\frac{r_h}{A}(\mathbf{N}(\rho_x^{\mathrm{e}})^{1/2}\right)\mathbf{B}_1 c^{\mathrm{e}}\right) \mathrm{d}\xi. \tag{62}$$

In the above expressions, the spherical differential operators,

$$\mathbf{B}_1 = r\frac{\partial \mathbf{N}}{\partial r} \quad \text{and} \quad \mathbf{B}_2 = \begin{bmatrix} r^2(\partial \mathbf{M}/\partial r) \\ 2r\mathbf{M}\end{bmatrix}, \tag{63}$$

and we used the constants $A$ and $H$ defined as

$$A = \frac{\left(2C_n\rho_p\right)^{1/2} l}{(\mathbf{N}(n_{\mathrm{s}})_{\mathrm{e}})^{1/3}(\bar{M}_n)^{1/2}} \quad \text{and} \quad H = 8\delta\tilde{\mu}_{\mathrm{f}}. \tag{64}$$

### 4.3 Numerical integration scheme and convergence

To obtain the time-dependent solution of hydrogel degradation, we now introduce a backwards Euler integration scheme that is used to solve the system of equation (49). The backwards Euler integration scheme approximates the value of one time step forward based on the approximate derivative at the next time step. This is written as follows:

$$\mathbf{d}_{t+\Delta t} = \mathbf{d}_t + \Delta t \dot{\mathbf{d}}_{t+\Delta t}, \tag{65}$$

where $\Delta t$ represents a numerical time increment. Owing to the inherent nonlinearity of the degradation problem, the solution for $\mathbf{d}_{t+\Delta t}$ is solved for iteratively at time increment $t + \Delta t$. The value $\mathbf{d}^i_{t+\Delta t}$ at the $i$th iteration is calculated by

$$\mathbf{d}^i_{t+\Delta t} = \mathbf{d}^{i-1}_{t+\Delta t} + \delta\mathbf{d}^i. \tag{66}$$

Combining and rearranging Equations (65) and (66), we computed the iterative displacement $\delta\mathbf{d}^i$ as

$$\left(\left(\frac{1}{\Delta t}\right)\mathbf{C}^t + \mathbf{K}^t\right)\delta\mathbf{d}^i = \mathbf{H}^i, \tag{67}$$

where $\mathbf{H}^i$ is the so-called residual vector, given by

$$\mathbf{H}^i = -\mathbf{b}_{nt+\Delta t} - \mathbf{C}^{i-1}_{t+\Delta t}\frac{\mathbf{d}^{i-1}_{t+\Delta t} - \mathbf{d}_t}{\Delta t}. \tag{68}$$

Iterations are then repeated until the norm of the residual $|\mathbf{H}^i| < \mathrm{tol}$, where tol is the tolerance. To complete the scheme, it is of interest to mention that the velocity $\dot{\mathbf{d}}^i_{t+\Delta t}$ at time $t + \Delta t$ and iteration $i$ is calculated as

$$\dot{\mathbf{d}}^i_{t+\Delta t} = \frac{\mathbf{d}^i_{t+\Delta t} - \mathbf{d}_t}{\Delta t}. \tag{69}$$

The convergence of the presented numerical scheme was assessed by plotting the norm of the residual vector $\mathbf{H}^i$ in terms of the iteration number $i$ for fixed term increment. As depicted in Figure 2(a), we observed a convergence that compared very well with quadratic convergence rate, as expected for the Newton–Raphson method.

Finally, it is important to mention that integrals (52)–(62) were numerically approximated using a Gaussian quadrature rule. In this context, the number of Gauss points per element is critical for obtaining optimal accuracy with maximum computational efficiency. For this reason, we studied the accuracy of the results by introducing an error measure as follows:

$$\mathrm{error} = \frac{\int_0^{R_{\mathrm{g}}}\left(c^{\mathrm{p}}(r) - c^{\mathrm{p}-1}(r)\right)\mathrm{d}r}{\int_0^{R_{\mathrm{g}}} c^{\mathrm{p}}(r)\,\mathrm{d}r}, \tag{70}$$

where $c^{\mathrm{p}}$ is the concentration profile at a given time increment, obtained using a $p$-point quadrature rule. The error was numerically calculated for 3, 4, 5, 6, 7 and 8-point quadrature rule for benchmark problems presented in the next section. Our convergence studies presented in Figure 2(b) showed that excellent accuracy was obtained for six Gauss points per element; this value was, therefore, chosen for the remainder of this paper.

## 5. Results and discussion

The proposed model is now used to examine how changes in polymer properties or enzyme choice affect degradation dynamics of hydrogels.

### 5.1 Enzymatic degradation of PEG hydrogels

The following application considers a hydrogel system made of polyethylene glycol (PEG) cross-linked system, previously described by Merrill et al. (1993), which fits well within the current assumptions of rubber elasticity theory, due to the simplicity of the cross-linked network. The gel under consideration is characterised by a linear polymer molecular weight of 35 kDa, an initial cross-linking density of 0.415 M (as calculated from the molecular weight between the cross-links) and an initial polymer volume fraction of 0.936 (Merrill et al. 1993). The PEG is assumed to have a Flory characteristic ratio,

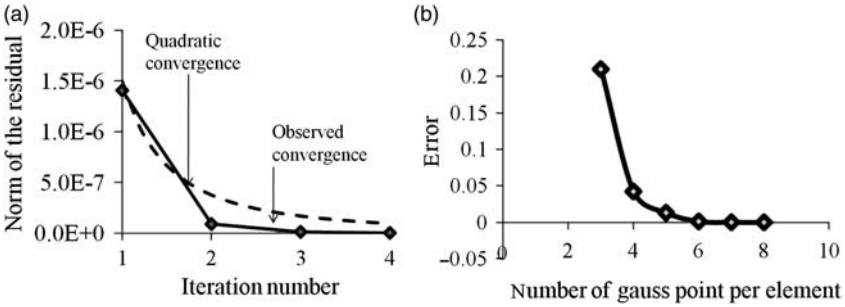


Figure 2. Convergence study. (a) Iteration convergence during a typical time increment. (b) Result accuracy in terms of the number of Gauss points used for numerical integration.

Table 3. Initial properties of the PEG hydrogel.

| Variable | Value | Equation number |
|---|---|---|
| $\mu$ (kPa) | 873.4 | (24) |
| $\xi$ (Å) | 88.4 | (29) |
| $p_{\text{osm}}$ (kPa) | 55.3 | (20) |

$C_n$ of 4, a Flory polymer–solvent interaction parameter, $\chi$, of 0.426 and a density $\rho_p$ of $1.204\,\text{g}\,\text{ml}^{-1}$ (Merrill et al. 1993; Bryant et al. 2004b) (PEG, Sigma-Aldrich, http://www.simaaldrich.com/catalog/). With the properties of PEG and the values given above, we calculated the properties of the polymer network, such as initial shear modulus, mesh size and osmotic pressure, using the constitutive relationships introduced earlier. These values are reported in Table 3.

To examine the kinetics of enzyme degradation and diffusion in the PEG hydrogel system, we chose enzyme characteristics based on relevant data from the literature. The Michaelis–Menton kinetic constants were selected to represent substrates that are highly susceptible to degradation by MMPs, enzymes secreted by many cell types. As a starting point, a $k_2/K_m$ value of $2.5E+0.5\,\text{M}^{-1}\,\text{s}^{-1}$ was selected (Chen et al. 2002). Specifically, the values of $K_m$ and $k_2$ used in the model was 189 $\mu$M and $47\,\text{s}^{-1}$, respectively. The hydrodynamic radius of the enzyme was estimated to be 20 Å (Merrill et al. 1993). Finally, enzyme is assumed to be released by cells at constant rate for which the magnitude follows from production studies done by Fahmi et al. (2001).

### *5.2 Numerical investigation of enzyme diffusion and gel degradation*

Preliminary observations of the trends exhibited by numerical simulations suggest that hydrogel degradation is characterised by a competition between the diffusion and degradation kinetics of enzyme molecules through the gel. If the degradation kinetics are dominated by diffusion (in this case, we refer to the system as *diffusion dominated*), enzyme diffuses through the gel faster than it degrades and a more uniform gel degradation is expected. However, if the kinetics of degradation dominate (in this case, we refer to the system as *degradation dominated*), gel degradation is expected to occur more locally. To better understand this behaviour, we introduce a scalar quantity, denoted as $\Phi$, which characterises the tendency of the system to be either diffusion dominated or degradation dominated. A good choice of $\Phi$ is given as follows:

$$\Phi = \frac{R_c^2 k_2}{D_g}. \tag{71}$$

In other words, $\Phi$ is defined as the ratio of degradation to diffusion rate (scaled by the size of the cell), in the initial gel configuration. Therefore, $\Phi$ becomes very large when the system is degradation dominated whereas $\Phi$ approaches zero when the system is diffusion dominated. Practically, the choice of $\Phi$ can be made by carefully selecting parameters defining enzyme and hydrogel (such as enzyme size to hydrogel mesh size, for instance). On the one hand, diffusion is strongly affected by a few initial parameters that include hydrodynamic radius of the solute and hydrogel mesh size. In real systems, the hydrodynamic radius can differ by targeting different enzymes released by the cell, whereas the mesh size can be controlled by designing hydrogel scaffolds with various initial cross-link densities. On the other hand, degradation kinetics are affected by both cross-link density (i.e. the more the cross-links, the slower the degradation) and by the chemistry of the cross-link which can lead to cross-links that are highly, moderately or minimally susceptible to degradation. These different design parameters directly affect the rate at which degradation occurs.

To assess the time evolution of enzyme diffusion and gel degradation for different types of systems, we investigated the profile of enzyme concentration and cross-link densities in terms of time for three values of $\Phi$ ($\Phi = 30, 1000$ and 8000), as presented in Figure 3. For this demonstration, the value of $\Phi$ was varied by manipulating the enzyme characteristics (enzyme size and $k_2$), while maintaining the same enzyme flux and

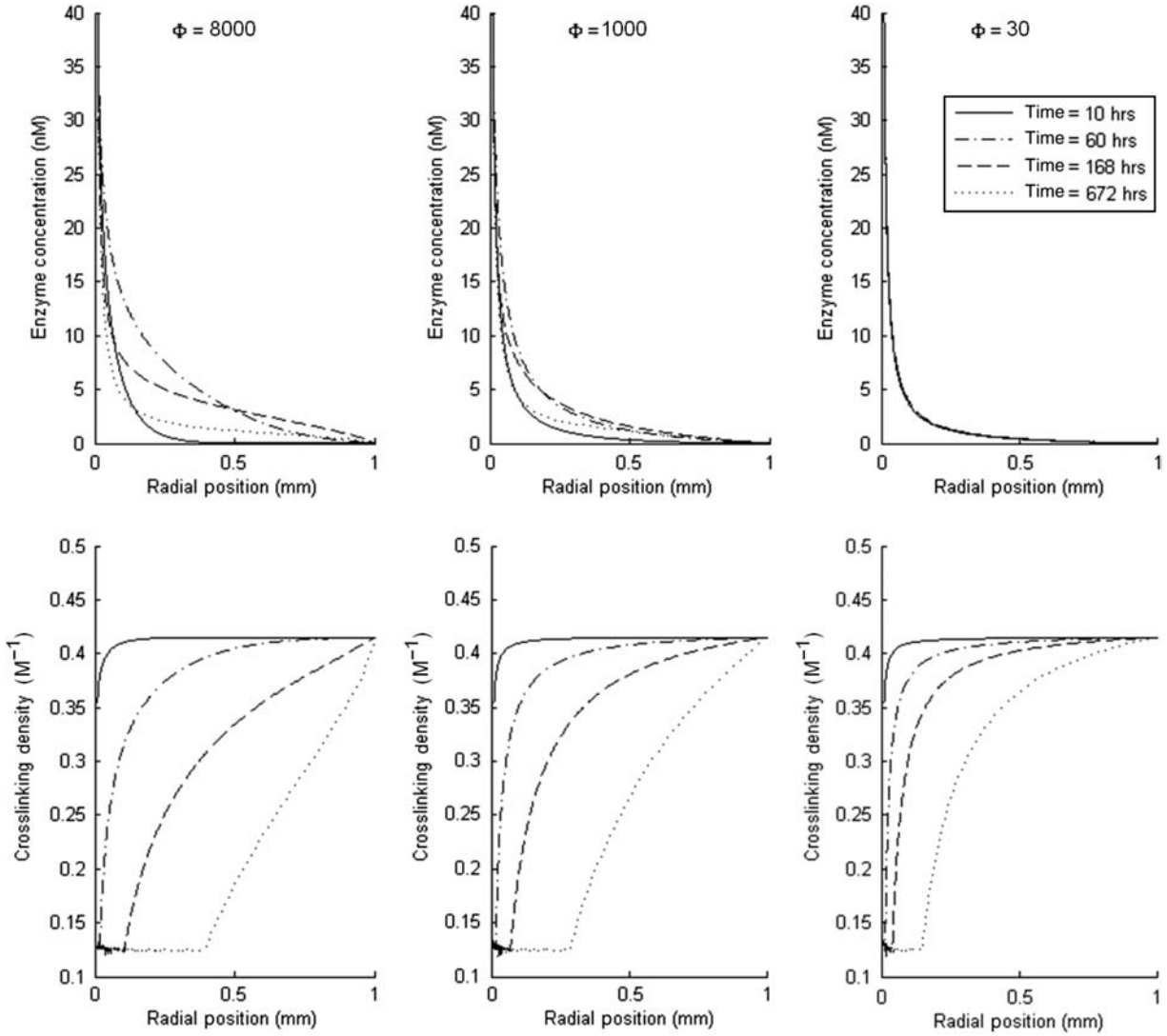


Figure 3. Evolution of the profiles of enzyme concentration and cross-link density for three values of $\Phi$ ($\Phi = 30, 1000$ and 8000).

initial cross-link density. In terms of the enzyme profile, we generally observe a high concentration near the cell followed by a rapid decrease with increasing radius away from the cell. Enzyme concentration diminishes to zero at $r = 1$ due to the boundary condition $c(1) = 0$. Furthermore, the profile of cross-link density permits one to visualise the spatial and temporal degradation behaviour of the hydrogel system. When $\rho_x$ is at its initial value (i.e. $0.41\,\mathrm{M}^{-1}$), the gel is not degraded, whereas when $\rho_x$ decreases to its maximum level of hydrogel degradation described by this model, corresponding to the point at which 60% of the cross-links have been degraded, the value of $\rho_x$ drops to $0.13\,\mathrm{M}^{-1}$. We generally observe degradation of the gel near the cell, due to the high enzyme concentration in this region. However, no gel degradation occurs at $r = 1$ as the enzyme concentration drops to zero at this location. A more thorough analysis of these results enables one to draw the following observations regarding the general behaviour of the system:

- *Degradation-dominated systems promote local gel degradation around cells through a bottleneck mechanism*. The evolution of cross-link density clearly shows that degradation evolves at a faster rate for large values of $\Phi$ (degradation dominated). This can be explained as follows: when $\Phi$ is large, there is fast degradation around the cell, in which enzyme concentration is high. In this degraded region, broken cross-links result in a larger polymer mesh size and thus a higher enzyme diffusivity. This creates a *bottleneck mechanism* in which a region of large diffusivity coexists with a region of low diffusivity further away from the cell. A large portion of the enzyme, therefore, accumulates and remains in the neighbourhood of the cell as can be

observed in the first plot of Figure 3 at 60 h. This mechanism greatly favours local degradation as compared with the diffusion-dominated systems.

- *Diffusion is not affected by degradation for diffusion-dominated systems*. By contrast to the previous observation, the evolution of enzyme concentration for low value of $\Phi$ shows that diffusion is unaffected by the level of gel degradation. This means that the added enzyme diffusivity due to degradation is not significant compared with the already very high initial diffusivity. In other words, enzyme can easily diffuse through the system, regardless of the level of degradation. This finding ensures that enzyme concentration stays relatively low in the gel (except in the immediate neighbourhood of the cell) and subsequently leads to a decrease in the rate of gel degradation.
- *The rate of global gel degradation increases with* $\Phi$. Referring to Figure 4, the rate of migration of the degradation front, which is defined as the region in which maximal degradation has occurred as defined by the model, increases as the value of $\Phi$ increases indicating an overall faster rate of degradation. As a result of the temporal changes in the local cross-link density, global changes in the hydrogel macroscopic properties are observed whereby gel swelling (shown by the radial displacement of a point located at $r = 1$) increases with $\Phi$ whereas the shear modulus decreases faster with time as $\Phi$ increases. These observations are consistent with the underlying mechanisms explained above.

Taken together, this model describes two distinctly different degradation regimes that may result from cell-mediated degrading hydrogels and which lead to spatial and temporal differences in the hydrogel structure and its global properties. Although the cell will largely dictate the degradation behaviour of the hydrogel, one can select the enzyme to target and manipulate the chemistry of the susceptible cross-link to favour either a diffusion-dominated system or a degradation-dominated system. For example, through simple variations in the peptide sequence, $k_2/K_m$ can vary over three orders of magnitude for the same enzyme (Chen et al. 2002). In designing degradable hydrogels for applications in tissue engineering, a system that favours a degradation-dominated mechanism is attractive in that it creates open space in the immediate region surrounding the cell for deposition of matrix macromolecules (e.g. collagen), which are typically too large to diffuse through cross-linked hydrogels (Bryant and Anseth 2003; Bryant et al. 2004a). As the degradation front grows, additional space is created for neotissue evolution. Alternatively, a diffusion-dominated system may be more attractive for strategies in which a slower and more general bulk degradation system is desired. In this kind of system, the cross-linking decreases on more of a macroscopic and global scale facilitating diffusion of smaller matrix molecules and thus promoting a more homogeneous development of neotissue.

## 6. Summary and conclusion

The triphasic mixture model presented in this paper is able to capture key processes driving cell-mediated enzymatic degradation of hydrogels. The contributions of this model are several folds. First, it captures the interactions between degradation and diffusion through a physically derived constitutive relation. Second, the incorporation of equilibrium swelling theory and rubber elasticity theory allows the mechanical and transport properties of the hydrogel to vary in both time and space. Model predictions have shown that diffusion and degradation in the hydrogel have a complicated relationship. Changes in diffusional characteristics not only changes the shape of the degradation front, but also changes the rate at which the whole system degrades. The major finding of the present analysis is that gel degradation is promoted by a system in which diffusion is resisted. For such degradation-dominated system, we found that the increased rate of

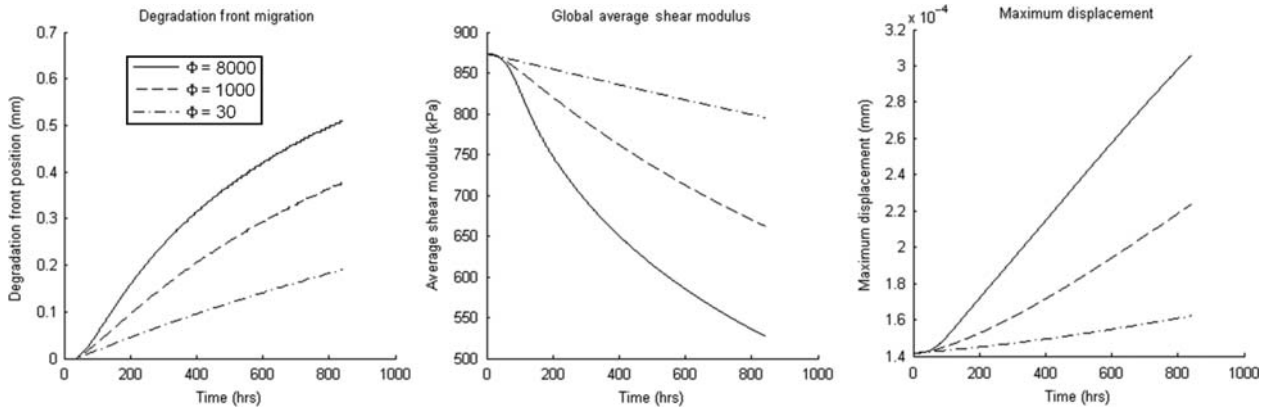


Figure 4. Evolution of degradation front, global shear modulus and gel swelling for different values of $\Phi$ ($\Phi = 30, 1000$ and 8000).

degradation can be attributed to the increased amount of enzyme retained in the hydrogel as the construct degrades.

Although this study only addresses gel degradation by cells, it will serve as a stepping stone onto which more elaborate studies can be built which combine gel degradation and matrix production by cells. The development of such a model will be invaluable in aiding the design of hydrogel scaffolds (to be used for *in vivo* tissue replacements) of which the degradation kinetics can be tailored to support physiological load while extra-cellular matrix is being produced by cells. In addition, the model is currently being validated with experimental procedures that aim to determine gel degradation by encapsulated enzyme-loaded microspheres. The comparison between experiments and model will be presented in a companion paper. In particular, the observation of real systems will provide critical insights into possible model improvements. Realistic improvements could for instance reside in a better description of the enzyme release by cells, the inclusion of the role of enzyme's half-life on gel degradation and the consideration of more realistic boundary conditions.

## Acknowledgements

FJV gratefully acknowledges the support of the University of Colorado CRCW Seed Grant and SJB acknowledges the support of NIH under grant K22DE016608. FJV and SJB greatfully acknowledge NIH grant number 1R21AR061011 in support of this work.

## Note

1. F.J. Vernerey and E.C. Greenwald contributed equally to this work.

## References

Anseth KS, Bowman CN, Brannon-Peppas L. 1996. Review: mechanical properties of hydrogels and their experimental determination. Biomaterials. 17:1647–1657.

Bell CL, Peppas NA. 1995. Biomedical membranes from hydrogels and interpolymer complexes. Adv Polym Sci. 122:125–175.

Biot MA. 1941. General theory of three-dimensional consolidation. J Appl Phys. 12:155–164.

Biot MA. 1957. The elastic coefficients of the theory of consolidation. J Astrophys Astron. 24:594–601.

Bowen RM. 1980. Incompressible porous media models by the use of the theory of mixtures. Int J Eng Sci. 18:1129–1148.

Bryant SJ, Anseth KS. 2003. Controlling the spatial distribution of ECM components in degradable peg hydrogels for tissue engineering cartilage. J Biomed Mater Res. 64A(1):70–79.

Bryant SJ, Bender RJ, Durand KL, Anseth KS. 2004a. Encapsulating chondrocytes in degrading peg hydrogels with high modulus: engineering gel structural changes to facilitate cartilaginous tissue production. Biotechnol Bioeng. 86(7):747–755.

Bryant SJ, Anseth KS. 2001. Hydrogel properties influence ECM production by chondrocyte photoencapsulated in poly(ethylene glycol) hydrogels. J Biomed Mater Res. 59:63–72.

Bryant SJ, Chowdhury TT, Lee DA, Bader DL, Anseth KS. 2004b. Crosslinking density influences chondrocyte metabolism in dynamically loaded photocrosslinked poly(ethylene glycol) hydrogels. Ann Biomed Eng. 32:1143–1149.

Chandrupatla T, Belegundu A. 2002. Introduction to finite elements in engineering. 3rd ed. Upper Saddle River, NJ: Prentice Hall.

Chen EI, Kridel SJ, Howard EW, Li W, Godzik A, Smith JW. 2002. A unique substrate recognition profile for matrix metalloproteinase-2. J Biol Chem. 277(6):4485–4491.

Elisseeff J, Anseth K, Sims D, McIntosh W, Randolph M, Langer R. 1999. Transdermal photopolymerization for minimally invasive implantation. Proc Natl Acad Sci USA. 96(6):3104–3107.

Fahmi H, DiBattista JA, Pelletier J, Mineau F, Ranger P, Martel-Pelletier J. 2001. Peroxisome proliferator-activated receptor $\gamma$ activators inhibit interlukin-1$\beta$-induced nitric oxide and matrix metalloproteinase 13 production in human chondrocytes. Arthritis Rheumatism. 44:596–607.

Flory PJ. 1941. Thermodynamics of high polymer solutions. J Chem Phys. 9(8):660.

Gobin AS, West JL. 2002. Cell migration through defined, synthetic extracellular matrix analogues. FASEB J. 16(3): 751–753.

Gu WY, Lai WM, Mow VC. 1999. Transport of multi-electrolytes in charged hydrated biological soft tissues. Transport Porous Med. 34:143–157.

Holmes MH, Mow VC. 1990. The nonlinear characteristics of soft gels and hydrated connective tissues in ultrafiltration. J Biomech. 23:1145–1156.

Horkay F, Tasaki I, Basser PJ. 2000. Osmotic swelling of polyacrylate hydrogels in physiological salt solutions. Biomacromolecules. 1(1):84–90.

Kim J, Park Y, Tae G, Lee KB, Hwang SJ, Kim IS, Noh I, Sun K. 2008. Synthesis and characterization of matrix metalloprotease sensitive-low molecular weight hyaluronic acid based hydrogels. J Mater Sci Mater Med. 19(11):3311–3318.

Kraehenbuehl TP, Zammaretti P, Van der Vlies AJ, Schoenmakers RG, Lutolf MP, Jaconi ME, Hubbell JA. 2008. Three-dimensional extracellular matrix-directed cardioprogenitor differentiation: Systematic modulation of a synthetic cell-responsive peg-hydrogel. Biomaterials. 29(18):2757–2766.

Lee SH, Moon JJ, Miller JS, West JL. 2007. Poly(ethylene glycol) hydrogels conjugated with a collagenase-sensitive fluorogenic substrate to visualize collagenase activity during three-dimensional cell migration. Biomaterials. 28(20): 3163–3170.

Levesque SG, Shoichet MS. 2007. Synthesis of enzyme-degradable, peptide-cross-linked dextran hydrogels. Bioconjugate Chem. 18:874–885.

Lustig SR, Peppas NA. 1988. Solute diffusion in swollen membranes. IX. Scaling laws for solute diffusion in gels. J. Appl. Polym. Sci. 36:735–747.

Lutolf MP, Hubbell JA. 2005. Synthetic biomaterials as instructive extracellular microenvironments for morphogenesis in tissue engineering. Nature Biotechnol. 23(1): 47–55.

Lutolf MP, Lauer-Fields JL, Schmoekel HG, Metters AT, Weber FE, Fields GB, Hubbell JA. 2003. Synthetic matrix metalloproteinase-sensitive hydrogels for the conduction of tissue regeneration: engineering cell-invasion characteristics. PNAS. 100:5413–5418.

Martens P, Anseth KS. 2000. Characterization of hydrogels formed from acrylate modified poly(vinyl alcohol) macromers. Polymer. 41(21):7715–7722.

Metters AT, Bowman CN, Anseth KS. 2000. A statistical kinetic model for the bulk degradation of PLA-b-PEG-b-PLA hydrogel networks. J Phys Chem B. 104: 7043–7049.

Merrill EW, Dennison KA, Sung C. 1993. Partitioning and diffusion of solutes in hydrogels of poly(ethylene oxide). Biomaterials. 14:1117–1126.

Nicodemus GD, Bryant SJ. 2008. The role of hydrogel structure and dynamic loading on chondrocyte gene expression and matrix formation. J Biomech. 41:1528–1536.

Park Y, Lutolf MP, Hubbell JA, Hunziker EB, Wong M. 2004. Bovine primary chondrocyte culture in synthetic matrix metalloproteinase-sensitive poly(ethylene glycol)-based hydrogels as a scaffold for cartilage repair. Tissue Eng. 10 (3–4):515–522.

Peppas NA, Barr-Howell BD. 1986. Characterization of the cross-linked structure of hydrogels. In: Hydrogels in medicine and pharmacy. Boca Raton, FL: CRC Press.

Rice MA, Sanchez-Adams J, Anseth KS. 2006. Exogenously triggered, enzymatic degradation of photopolymerized hydrogels with polycaprolactone subunits: experimental observation and modeling of mass loss behavior. Biomacromolecules. 7:1968–1975.

Sengers BG, Donkelaar CCV, Oomens CWJ, Baaijens FPT. 2004a. The local matrix distribution and the functional development of tissue engineered cartilage, a finite element study. Ann Biomed Eng. 32:1718–1727.

Sengers BG, Oomens CWJ, Baaijens FPT. 2004b. An integrated finite-element approach to mechanics, transport and biosynthesis in tissue engineering. J Biomech Eng. 126: 82–91.

Shu XZ, Liu YC, Prestwich GD. 2006. Osteochondral defect repair with autologous bone marrow-derived mesenchymal stem cells in an injectable, *in situ*, cross-linked synthetic extracellular matrix. Tissue Eng. 12(12):3405–3416.

Sun DN, Gu WY, Guo XE, Lai WM, Mow VC. 1999. A mixed finite element formulation of triphasic mechano-electrochemical theory for charged, hydrated biological soft tissues. Int J Numer Methods Eng. 45:1375–1402.

Tibbitt MW, Anseth KS. 2009. Hydrogels as extracellular matrix mimics for 3D cell culture. Biotechnol Bioeng. 103(4): 655–663.

Trusdell C, Noll W. 1965. Non-linear field theories of mechanics. Handbuch des Physik. Berlin: Springer. p. 537–541.

Vernerey FJ, McVeigh C, Liu WK, Moran B, Tewari D, Parks D, Olson G. 2006. The 3-D computational modeling of shear-dominated ductile failure in steel. J Minerals Metals Mater Soc. 433–445.

Vernerey FJ, Liu WK, Moran B. 2007a. Multi-scale micromorphic theory for hierarchical materials. J Mech Phys Solids. 55:2603–2651.

Vernerey FJ, Liu WK, Moran B, Olson G. 2007b. A micromorphic model for the multiple scale failure of heterogeneous materials. J Mech Phys Solids. 56: 1320–1347.